Automated high-content image-based characterization of microorganism behavioral diversity and distribution

Carlotta Aurora Lupatelli
Université Côte d'Azur
Agnès Attard
National Research Institute for Agriculture, Food and Environment
Marie-Line Kuhn
National Research Institute for Agriculture, Food and Environment
Celine Cohen
Université Côte d'Azur
Philippe Thomen
Université Côte d'Azur
Xavier Noblin
French National Centre for Scientific Research
Eric Galiana (eric.galiana@inrae.fr)
National Research Institute for Agriculture, Food and Environment

Method Article

Keywords: Microorganisms, micro-environments, drivers, distribution, automated image analysis, cell tracking

Posted Date: July 19th, 2023

DOI: https://doi.org/10.21203/rs.3.rs-3167274/v1

Additional Declarations: No competing interests reported.

Automated high-content image-based characterization of microorganism behavioral diversity and distribution

Carlotta Aurora Lupatelli[1,2], Agnes Attard[1], Marie-Line Kuhn[1], Celine Cohen[2], Philippe Thomen[2], Xavier Noblin[2], Eric Galiana[1*]

[1*]Université Côte d'Azur, INRAE, CNRS, ISA, Sophia Antipolis, 06903, France.
[2*]Université Côte d'Azur, CNRS, UMR 7010, INPHYNI, 06200, France.

*Corresponding author(s). E-mail(s): eric.galiana@inrae.fr;
Contributing authors: carlotta.lupatelli@inrae.fr; agnes.attard@inrae.fr; marie-line.kuhn@inrae.fr; celine.cohen@unice.fr; philippe.thomen@unice.fr; xavier.noblin@unice.fr;

Abstract

Background
Microorganisms evolved complex systems to respond to environmental signals. Gradients of particular molecules alter microbe behavior and distribution within their environment. Microdevice tools coupled to automated image-based methods are now employed to analyze instantaneous distribution and motion behaviors of microbial species in controlled environments at small temporal scales, mimicking to some extent macro conditions. Such technologies have already been adopted for investigations mainly on individual species. Similar versatile approaches must now be developed for the characterization of multiple and complex interactions between the microbial community and environment.

Results
Here, we provide a comprehensive step-by-step method for the characterization of species-specific behavior of a synthetic mixed microbial suspension in response to an environmental driver. By coupling accessible microfluidic devices with automated image analysis approaches, we evaluated the behavior response of three morphologically different telluric species (*Phytophthora parasitica, Vorticella microstoma, Enterobacter aerogenes*) to a potassium gradient driver. Using the TrackMate plug-in algorithms, we performed morphometric and then motion analysis to characterize each microbial species response to the driver. Such approach enabled us to confirm the different shape features of the three species, and to simultaneously characterize their particular motion adaptation to the driver, as well as their co-interaction dynamics.

Conclusions
The results obtained demonstrated the feasibility of the method to screen mixed-species suspension dynamics at high spatial and temporal scale. By increasing the complexity of suspensions, this approach could be integrated to support conventional omics methods, contributing to characterizing how the main drivers operate at the microbiota- host-environment interfaces. In its current advances, the method can integrate screening strategy, for example, for biocontrol agents evaluation, enlightening possible beneficial-pathogenic interactions based on co-colonization of micro habitats.

Keywords: Microorganisms, micro-environments, drivers, distribution, automated image analysis, cell tracking

Background

Microbiomes are shaped primarily by the environment and biotic interactions. In ground ecosystems, soil parameters (i.e. pH, soil texture, mineral fluxes) and soil management appear to be the main drivers for the composition and dynamics of telluric microbiomes[1]. Depending on soil properties and uses, the microbial dynamics may vary significantly on large time scales (the scale of years, months, and days). Over the last decades, various approaches have been developed to explore how and which drivers affect soil microbial dynamics at these different large time scales [2, 3].

For example, substantial monthly variability has been revealed between land use types using 16S ribosomal RNA amplicon sequencing [4]. Time sequences occurring at much shorter scales were also investigated. Daily moment events taking place in small soil volumes have been examined for characterizing drivers regulating intensive process rates and interactions [2]. The development of a rhizosphere-on-a-chip system coupled with the determination based on mass spectrometry of exudate metabolites allowed the definition of rhizospheric hotspots of exuded amino acids detected from 2 hours to 12 days and to which some soil microorganisms may converge to form a microbiota [5]. The second to minute range is also crucial to understand how dispersion, latent stage versus germination of spores, or displacement and guidance of swimming cells are regulated by these ways to the spatial dynamics and distribution of soil microorganisms [6–8]. Within this time slot, microorganisms may sense and respond to a variety of physical and (bio)chemical stimuli, such as light, electric fields, and nutrient availability [8].

The "instantaneous" distribution and growth of each microbial species is determined according to its ability to respond to changes in the environment, or succeeding or not to sense and then reach nutrients or a host in the case of pathogens and symbionts. Therefore, in this short and immediate time range, different and complex drivers determine the distribution and composition of microorganism populations in various hotspots (habitats). To characterize drivers operating on this time scale, the development of microfabrication offers the opportunity to design geometrically defined microdevices targeted for the analysis *in situ* of low volumes of microbial samples [9]. Precision environmental control typical of microfluidic circuits coupled to automated cell tracking and image analysis has already allowed quantification of microbial dynamics on a high spatial

and temporal resolution scale guided by particular soil drivers, including soil or plant derivatives [10, 11]. Progress in automated cell tracking was also recently achieved with the introduction of deep learning-based object tracking, improving performance, usability, and versatility, such as the TrackMate program (version 7.0.0) within the Java image processing program Fiji [12–14].

A challenge is now to begin to characterize the effect of a driver, not only on cells of a single species but also on more complex synthetic microbial consortiums to mimic, to some extent, a microbiota. This should lead to a better understanding of how microbial dynamics and diversity are regulated at microscales by testing hypotheses of the role of known drivers in the distribution of various microorganisms in a particular habitat.

Here, we implement coupled microfluidic technologies to automate cell tracking to investigate the behavioral response of three different telluric species within a synthetic community to a spreading driver, a controlled potassium gradient. In the soil, potassium efflux can be generated by rhizospheric activity, soil exchange dynamics, and / or release from the microbiota sharing the same biotope [15].

In our case, we evaluated the chemotactic effect of potassium gradient on *Phytophthora parasitica* zoospores, *Vorticella microstoma* protozoa cells and *Enterobacter aerogenes*. *Phytophthora parasitica* is a filamentous eukaryotic plant pathogen, causing disease in natural and agricultural systems worldwide, and spreading in water films by biflagellate zoospores known to respond to potassium gradient by negative chemotaxis [11, 16]. *Vorticella microstoma* is a suspension-feeding ciliate living in freshwater and soil habitat, in two forms: free-swimming telotroch and sessile stalked trophont [17]. Sessile stalked trophonts are suspension-feeding forms, using oral cilia beat to generate water vortex flow to draw bacteria feeding particles toward a mouth-like part, the peristome [17, 18]. *Enterobacter aerogenes* is a gram-negative motile bacteria, associated with a variety of environmental habitats [19], including soil [20], where they can act as endophytic plant bacteria [21]. The choice of using the three stains was determined by different factors. The different sizes of *P. parasitica* zoospores, *V. microstoma* ciliates and *E. aerogenes* bacteria cells (diameter above 10, 30 and 2 μm, respectively), were suitable to easily detect the species and follow their distribution upon microscope visualization. In the same way, the well-known response of *Phytophthora* zoospores to the potassium gradient was appropriate evidence for following and confirm automated cell tracking analysis.

From a biological perspective, the methodology implied was particularly interesting to study the co-occurrence of the three species. Possible co-evolution of related species within the same rizospheric environment was previously reported,

as well as the ability of *P. parasitica*, *Enterobacter* sp., and *Vorticella* sp. to constitute a mixed species biofilm [22, 23].

Methods

We applied morphometric analyzes and performed single cell tracking to first identify the three species in suspension and later discriminate their specific environmental response. We applied an image-based method for visualization and characterization at a species-specific level of the behavior and micro-distribution of three different microbial species in a mixed synthetic cell suspension at high temporal and spatial resolution upon a driver (Additional File 1). The application of this workflow might integrate the description of the complex microbial dynamics within humid soils or aquatic habitats, in support of classical omics approaches.

Oomycete, ciliate and bacterial strains

Phytophthora parasitica (isolate 310) was obtained from *Phytophthora* INRAE collection (Sophia Antipolis). *Vorticella microstoma* 30897 and *Enterobacter aerogenes* 13048 strains were purchased from the American Type Culture Collection (ATCC).

Culture conditions and synthetic community cell suspension

Phytophthora parasitica was cultured on malt agar at 24°C. Mycelia were cultured for one week in V8 liquid medium at 24°C under continuous light. The material was then dilacerated and incubated for a further four days on 2% agar in water. The zoospores were released as described by Larousse et al. (2014) [24]. *Vorticella microstoma* and *Enterobacter aerogenes* cells were cultivated for 3 to 4 days in V8 liquid medium at 24°C with a 16-h photoperiod. Ciliate and bacterial cells suspended in liquid medium were separated from the flocculates through a 15 min decantation step of 10 mL of the culture and recovery of the upper 0.5 mL. The mixed suspensions of *P. parasitica* (P), *V. microstoma* (V) and *E. aerogenes* (E) cells were generated in water and calibrated about 200, 10 and 2000 cells/μl, respectively.

Set-up used for cell motion analysis

Each P-V-E cell community suspension (50 μl) was placed in a microchamber (μ-Slide VI—flat; Ibidi; size l: 17 mm; w: 3.8 mm; h: 400 μm). A passive dispersion system was used to generate an environmental gradient of potassium by adding 0.5 μl of 500 mM KCl to a lateral open inlet [11]. At the 5 min time point, cell motion was captured with an Axio Imager Z1 microscope (Zeiss)

equipped for bright-field microscopy. The Axiovision 4.6 software (Zeiss), generating sequences of 10 s at a frame interval of 0.07350 s, controlled acquisition movies (Additional File 2; Additional File 3; Additional File 4).

Image treatment

Image pre-treatment and analysis were performed in a Fiji software environment [12]. To facilitate the comprehension of the manuscript when referring to the microbial cells, we use the term spots or objects, in line with Fiji language. Three different movies corresponding to three different biological replicates were first converted into an 8-bit color graphic and reported with the correct size scale. Each movie was then transformed into a mask of binary images where regions of interest (ROIs) corresponding to biological objects were converted into black spots (pixel value=255) over a white background (pixel value=0). The threshold values applied to obtain such binary images varied between 100 and 118 and were properly adapted to each specific situation (i.e., different objects or different pixel values on original grayscale images). We then proceeded to the analysis of cell motion dynamics, as reported below at millimetric and micrometric scales. In the latter case, to better define the micrometric areas to analyze, we created different reference grids for each replicate composed of squares with approximately 170-μm side.

Automated cell-image analysis

Morphometric and motion dynamics data were generated as follows. Dynamics of cell motion were investigated using TrackMate version 7, integrating algorithms for display and quantifying the shape of objects in 2D and 3D [14]. Under the TrackMate environment, objects are analyzed by two operational modules, a first one which allows the detection and filtering of the present objects, or spots, and a second one during which a tracker module links together the filtered spots to build tracks. Here, to detect and filter spots of interest into the previously obtained binary masks, we selected mask detector 2D option which results in the individualization of all spots by delineating each different perimeter and calculating areas or shape scores. The mask detector creates objects from a black and white channel in the 8-bit source image, based on the pixel having values strictly larger than 0. To allow the distinction and separated analysis of each biological object, we set the parameters of the Mask detector as follows: initial threshold adjusted at 1 in all three cases; radius of spots (accessible through set filters on spot) with a threshold above values included between 10 and 13.5 μm for *Vorticella* (V) and below values included between 2 and 4.5 μm for *Enterobacteria* (E). In the case of *Phytophthora zoospores* (P), we set the radius filter twice on the spots. In the first filtering we selected

spots with a radius below values 10-12 μm, in order to exclude *Vorticella* objects; in the second we selected a radius presenting values above 4-5 μm, to distinguish zoospores from bacteria cells. Tracking of trajectories was performed through Nearest-neighbor tracker algorithms, which links spots frame to following frame, by minimizing the global displacement of the particles. In the tracking settings, we tested different maximal linking distance values to be able to visually distinguish the trajectories of the three types of cells. We finally adopted maximal linking values of 15 μm for P, 60 μm for V and 2 μm for E, knowing that the fastest expected species was *V. microstoma* and the slowest was *E. aerogenes*. From the resulting analysis tables automatically generated by TrackMate, we extrapolated and plotted estimations related to area and perimeter of spots associated with each trajectory, to morphologically identify the three species, and to calculate mean speed of cells, in order to analyze their specific behavioral response. In the particular case of cell motion analysis at micrometric scale, we proceeded with mean speed and confinement ratio (persistence) measurements. Confinement ratio is defined as the ratio between the net displacement and the total distance travelled by each spot, so here by each microbial cell [25]. Hence, values close to 0 indicate a confined movement, where microbial particles remain close to the starting point of their path or displacement. Values close to 1, indicate that microbial particles are moving away from the starting point of the track with constant orientation. Statistical analysis was performed using a one-way analysis of variance (ANOVA) test with a Sidak post hoc test for multiple comparisons (GraphPad Prism version 10, GraphPad Software, Boston, Massachusetts USA).

Results

Morphological discrimination of the three species

Detection of spots through the TrackMate detector's Mask detector allowed the discrimination of three different groups of spots according to the expected estimate of the area and perimeter of the three microbial cells. The total number of spots for each group corresponded to the sum of spots detected in each frame over three movies replicate, resulting in a total of 430 frames (Table: 1). The first group of detected spots included 129952 spots corresponding to *P. parasitica* zoospores (Fig.1c), exhibiting area and perimeter values between 50-200 μm^2 and 30-100 μm , respectively (Fig.2a-2b). A second group, counting 4532 spots, corresponded to *V. microstoma* cells. The protozoa cells presented the highest area and perimeter values, with the majority of the spots having values ranging between 400-1000 μm^2 and 100-200

μm of area and perimeter, respectively (Fig.2a-2b). The heterogeneity in size shape was clearly associated to the free-swimming or sessile status of the ciliate cells, with large motile cells detected as ellipsoidal and smaller non-motile cells detected as circular spots (Fig.1d). Circularity parameters retrieved from TrackMate table further confirmed the double-shape status of *V. microstoma*. Only a minority of protozoa cells presented values closer to 1, corresponding to the more circular sessile forms of the ciliate, while the majority of cells had values between 0 and 0.5, more likely to represent its ellipsoidal like free-swimming forms (Fig.2d).The third group included the smallest detected spots associated to *E. aerogenes* cells (Fig.1e), with a 60% of detected spots having an area of approximately 12 μm^2 as maximum and almost the 75% of spots having a perimeter included between 0-15 μm (Fig.2a-2b). Bacteria cells also represented the largest number of microbial organisms within the suspension analyzed (744475 spots).

Distribution and behavioral response of P, V and E to potassium gradient at millimetric scale

A passive dispersion system generated by adding the potassium solution to the lateral open inlet of the microchamber, was used to investigate motion responses of the three different microbial species. The point of potassium inclusion, thus corresponding to the area that maintained the maximum concentration of the ion throughout the observation, corresponded to the upper side of the resulting images (Fig.1a). To describe the motion dynamics adopted by the microbial species after 5 minutes of potassium diffusion, we defined the trajectories and mean speed values for each species (Fig.1f-1g-1h; Fig.2c). Short trajectories indicate spots (microbial cells) traveling short distances or part of long trajectories not entirely tracked by the TrackMate Fiji plug-in. Non-motile spots are normally represented within their profile shapes and do not display any trajectory pattern (Fig.1f-1g-1h).

As expected, *P. parasitica* zoospores (12744 tracks) occupied the millimetric space heterogeneously, displaying the characteristic negative chemotaxis towards the potassium gradient (Fig. 1a) [11]. The net linear trajectories were mostly delineated in the area below the potassium inclusion point, while only a few apparently nearly immobile forms (null or short trajectories) were detected in the vicinity of the same micro-area (Fig. 1f). The mean speed distribution of the zoospores also defined two different motion patterns, with a minority of cells with a mean speed included between 4-20 $\mu m/s$ and a majority with mean speed values between 100-200 $\mu m/s$

	Microbial Species	Number of spots	Number of Tracks	Area μm^2 [min-max]	Perimeter μm [min-max]	Mean speed $\mu m/s$ [min-max]
Replicate 1 (143 frames)	*P. parasitica*	26966	2918	[79-360]	[37-198]	[0-213]
	V. microstoma	973	32	[451-1500]	[101-256]	[2-540]
	E. aerogenes	326387	31004	[2-56]	[6-67]	[0-28]
Replicate 2 (143 frames)	*P. parasitica*	44713	4189	[48-340]	[26-141]	[0-210]
	V. microstoma	2271	73	[354-2485]	[84-169]	[1-760]
	E. aerogenes	275901	24843	[2-25]	[6-33]	[0-28]
Replicate 3 (144 frames)	*P. parasitica*	58273	5637	[46-239]	[25-165]	[0-211]
	V. microstoma	1288	43	[397-1892]	[73-335]	[2-648]
	E. aerogenes	14187	24975	[2-32]	[8-43]	[0-28]

Table 1 Replicates analyzed for morphometric and motion observations. For each replicate, the three microbial species presented different numbers of spots and tracks detected, and calculated uniform mean values of the considered parameters (area, perimeter, mean speed). *V. microstoma* presented a limited number of cells and tracks.

(Fig 2c). *Phytophthora parasitica* zoospores with null trajectories and very low mean speed values (below 10 $\mu m/s$) were considered as effectively non-motile (Fig. 1f) (Fig. 2c).

Similarly, over a total of 148 tracks, also *V. microstoma* cells displayed mean speed values distributed mainly over two intervals, with approximately the 30% of spots having a mean speed within 20-60 $\mu m/s$ and the rest values included between 80-800 $\mu m/s$ (Fig. 2c). On the contrary, protozoa cell trajectories appeared uniformly distributed with a linear pattern along the entire millimetric environment analyzed, without exhibiting significant spatial preference in relation to the KCl gradient (Fig. 1g). *Vorticella microstoma* cells with null trajectories and mean speed metrics below 20 $\mu m/s$ were considered corresponding to the sessile forms of protozoa, while all others with higher mean speed metrics and longer trajectories pattern were considered and easily characterized in the movies as the protozoa free-swimming telotroch forms (Fig.1g) (Fig.2c).

Bacterial cells (80822 tracks), finally displayed mainly two different types of trajectories, a more curved and circular-like trajectory in the proximity of *V. microstoma* sessile forms, and a more linear and shorter trajectory in the surrounding area (Fig.1h). The bivalent bacteria displacement pattern occupied the entire millimetric space, regardless of proximity or no proximity to higher potassium concentrations. The majority of bacterial cells ($< 40\%$) displaced at a very low mean speed below 20 $\mu m/s$ (Fig.2c).

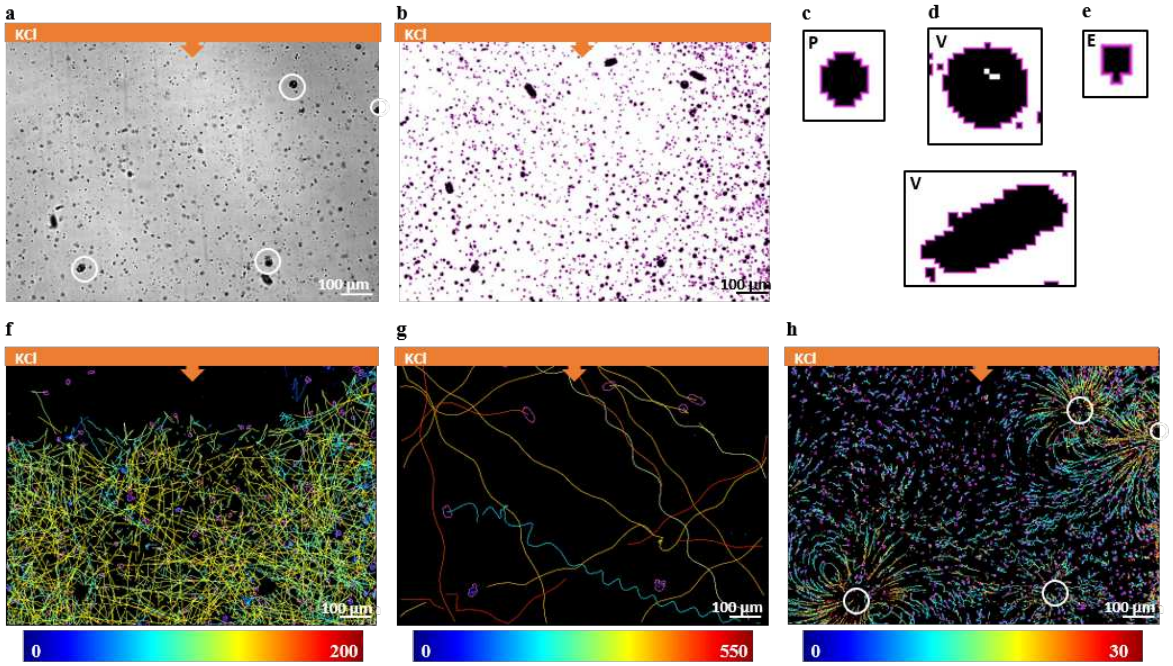

Fig. 1 Detected spot shapes and trajectory patterns of the three different microbial species upon potassium gradient. (1a) A representative overview of the original frames. Potassium solution (KCl) diffused passively from the inclusion point indicated by the orange bar on the top of the image. (1b) Mask detector delimitated the shapes of the three different morphological spots on the transformed binary frames. (1c) Shapes of *P. parasitica* zoospores (P) associated spots. (1d) Circular shapes associated to sessile forms of *V. microstoma* (V) on the top; ellipsoidal shapes associated to free-swimming forms of *V. microstoma* (V) on the bottom. (1e) Detected spot shapes associated to *E. aerogenes* cells (E). (1f) The confined trajectory pattern of *P. parasitica* zoospores revealed a negative chemotactic behavior in response to potassium gradient with optimal conditions for swimming away from higher concentrations. (1g) *V. microstoma* exhibited mostly linear or sinusoidal trajectories. Sessile forms, encircled in 1a and 1h, did not display any trajectory. (1h) Trajectories of *E. aerogenes* in proximity or not to sessile *V. microstoma* with characteristic patterns of vortex flows around sessile *Vorticella* forms. At the bottom of the 1f, 1g, and trajectories images is the corresponding mean speed ($\mu m/s$) color bar, varying from blue/green (low speed) to yellow/red (high speed). Movies were obtained at 10x magnification and analyzed in Fiji environment. Scale bars: 100 μm.

Analysis of motion behavior at micrometric scale revealed other environmental interactions

A systematic screening of the movies at a micrometric scale was performed to further analyze the properties of the synthetic microbial community suspension using a grid with an area unit of $170 \times 170\ \mu m^2$ associated to a correlation code of letters and numbers (Fig.3a-3b). At this resolution, the study allowed us to identify two distinct motion behaviors for each species, occurring in particular micro-environment areas.

In the most evident cases of *P. parasitica* and *E. aerogenes*, we were able to discriminate and further investigate their motion behaviors in two micro-environments where P was subjected or not to KCl gradient, and E was in proximity or not to *V. microstoma* sessile forms. For

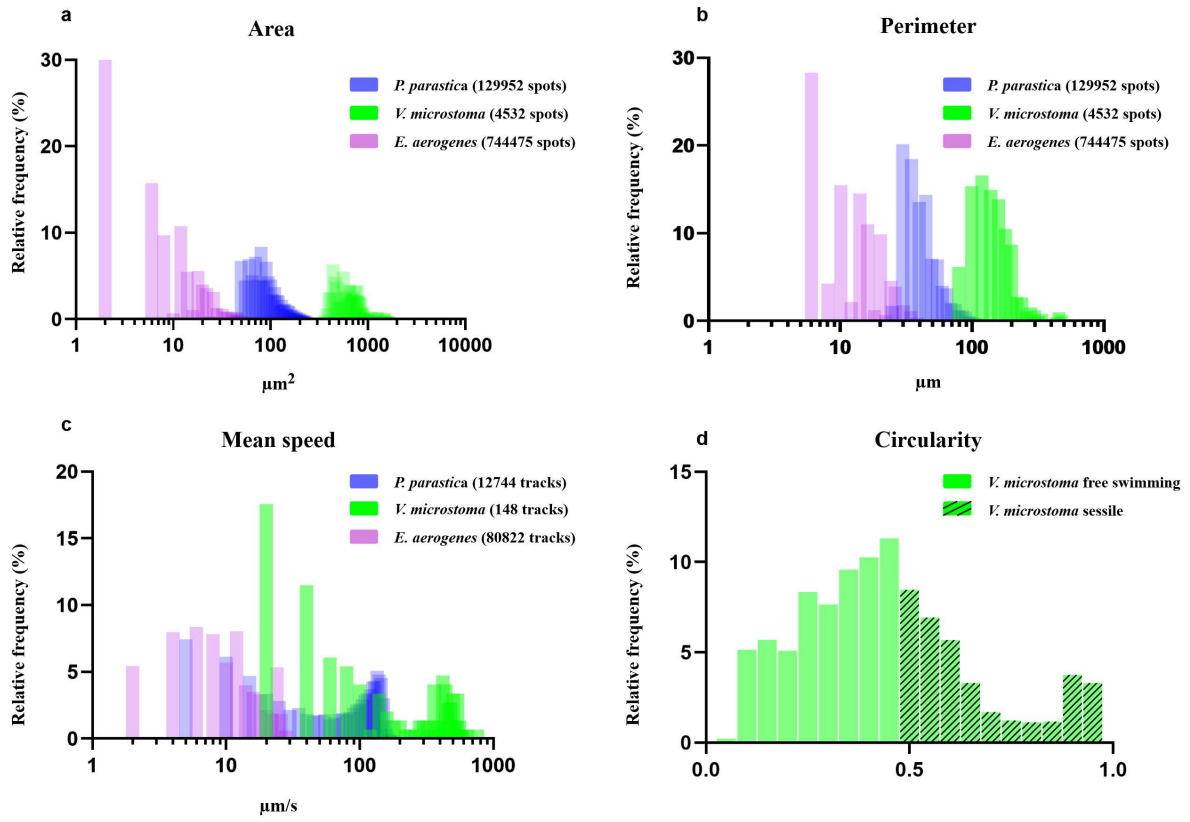

Fig. 2 Frequency distribution of morphometrics and motion characterizing the three microbial groups.(2a,b,c) Frequency distribution of areas (2a), perimeters (2b) and mean speeds (2c) of the three species based on data merged from the three replicates. *V. microstoma* resulted to be the largest and fastest species in the suspension while *E. aerogenes* the smallest and slowest. On the y axis, the relative frequency in percentage (%), on the x axis the area, perimeter, and mean speed measurements (μm^2, μm and $\mu m/s$) adapted to a log10 scale. (2d) Frequency distribution of circularity values for *V. microstoma* cells (data merged from the three replicates). Values included between 0.5 and 1 indicate the more circular *V. microstoma* sessile forms. On the y-axis, the relative frequency in percentage (%), on the x axis, the circularity interval.

Vorticella microstoma, we deliberately defined a micro-environment characterized by the presence of V sessile forms and one characterized by V free swimming forms. As a result, for each replicate, six different micro-environments were established (Table 2) (Fig. 3c-3d-3e-3f-3g-3h).

To normalize our observations, we tried to select for each micro-environment same number of grid cells for each species in each replicate. For each species, we analyzed the same number of frames (Table 2), within the same replicate. The frames selected were based on the best spatial and temporal placement, so that no interference with the other microorganisms in suspension or other micro-environment occurred. For each micro-environment we analyzed mean speed and confinement ratio values of the three species in order to describe their distinct motion dynamics (Fig.4).

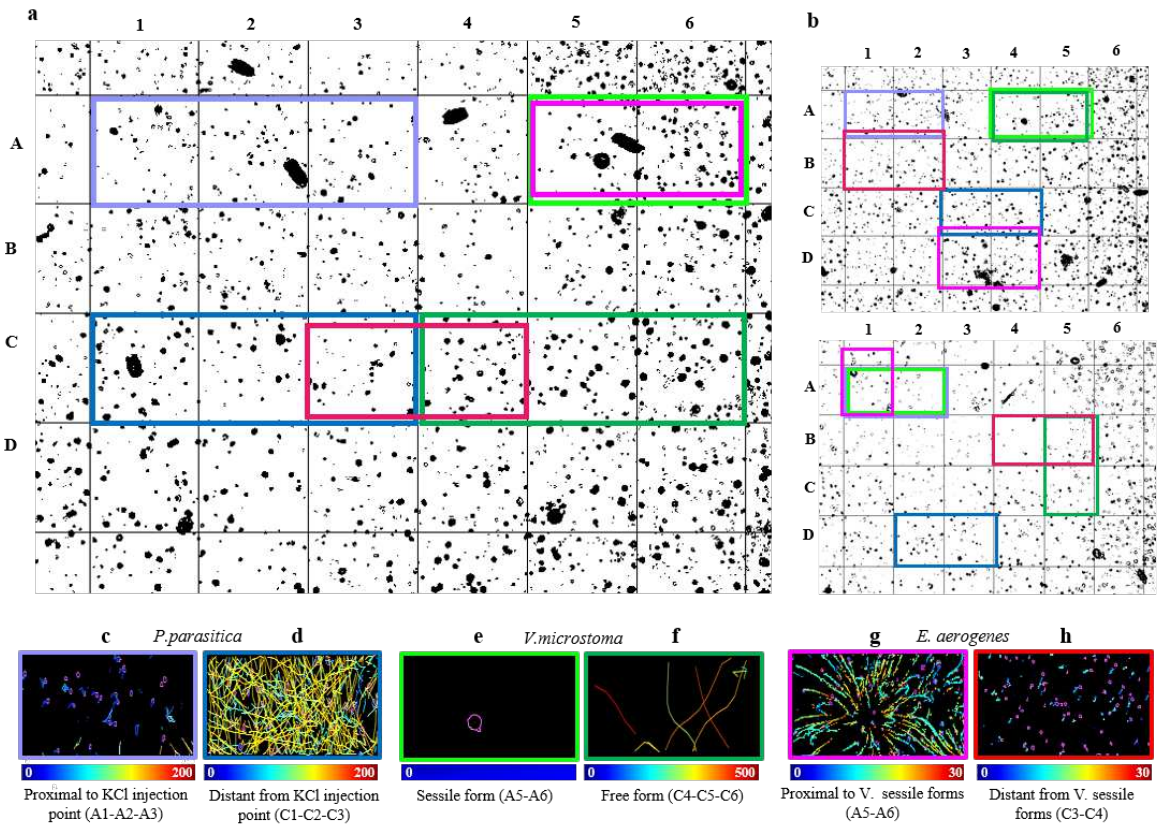

Fig. 3 Definition of six different micro-environments based on trajectory patterns. (3a) Example of grid applied to replicate 1. Labeled in different colors, the grid cells correspond to each micro-environment. The labeling code is shown in 3c. (3b) Grid applied to the other two movies replicates and respective colored labels. (3c,d,e,f,g,h) Trajectory patterns for six different micro-environments in replicate 1: from the right *P. parasitica* (proximal to KCl injection point vs. distant from KCl injection point) from A1-A2-A3 cells and C1-C2-C3 cells; *V. microstoma* analysis (sessile vs free swimming forms) from A5-A6 and C4-C5-C6 cells; *E. aerogenes* analysis (in proximity of *V. microstoma* (V) sessile forms vs. distant from V sessile forms) from A5-A6 and C3-C4 cells. Below each image, a bar color code for the range of mean speeds ($\mu m/s$).

Micro-environment analysis revealed that *Phytophthora parasitica* zoospores showed for each replicate two different sets of mean speed values (ANOVA test ($p < 0.0001$)) depending on the proximity (Fig.3c), or not (Fig.3d), to the generated potassium gradient (Fig.4a). In the micro-environment where the zoospores were subjected to negative potassium chemotaxis, moving away from the potassium injection point, the mean speed value for the three replicates was higher, with values above 50 $\mu m/s$ (Fig.4a). In replicates 1 and 2, most zoospores reached a velocity of 150 $\mu m/s$, while fewer zoospores belonging to replicate 3 reached the same value (Fig.4a) suggesting the presence of a higher number of non-motile forms of zoospores. Conversely, mean speed values dropped to 0 $\mu m/s$ when zoospores were moving in the micro-environment corresponding to highest potassium concentration (micro area around the injection point) (Fig.4a). Non-motile

zoospores exhibiting low mean speed values corresponded to their de-flagellated and encysted forms previously described in the literature in the presence of a high concentration of potassium [16].

Mean speed analysis of the two micro-environments associated with *V. microstoma* revealed values mostly above 400 $\mu m/s$ for long trajectories of free-swimming forms of protozoa and approximately between 0-50 $\mu m/s$ for sessile forms (Fig. 3d-3e) (Fig.4c), independently of their proximity or not to the injection point of KCl. Subaverage mean speed ranges (spanning down to 0 $\mu m/s$) found in the micro-environments of the free-swimming *V. microstoma* forms of replicate 2 and 3 (Fig.4c), are explained by the copresence of a sessile form of the same species within the considered frames. Considering limitations of ANOVA statistical test for small sample size, we did not perform any statistical test for *V. microstoma* cells group, which counted overall only 24 total tracks (Table 2).

The investigation of the two micro-environments associated to *E. aerogenes* behavior revealed two sets of mean speed values: one related to bacteria located far from *V. microstoma* sessile forms (Fig.3h) with mean speed values on average below 10 $\mu m/s$, and a second related to bacteria located close to *V. microstoma* sessile forms with a higher mean speed (on average above 10 $\mu m/s$) (Fig.3g) (Fig.4e). The results were further confirmed by the ANOVA statistical test, showing the difference between the two conditions tested ($p < 0.0001$). In line with millimetric observations, we again appreciated more circular trajectories of bacteria near and around the sessile protozoa forms, and shorter and straight trajectories for bacteria more distant from sessile protozoa forms (Fig.1h). Together, these circular bacterial trajectories formed a circular vortex resulting from the water flow dragging force generated by the oral cilia beating of *V. microstoma* sessile trophont forms [17].

For each micro-environment and estimated cell tracks, we also calculated confinement ratio rates. ANOVA statistical tests were further performed only for *P. parasitica* and *E. aerogenes* groups. As expected, values mostly distributed closer to 0 were recorded for *P. parasitica* zoospores close to potassium injection point (Fig.4b) and immobile forms of *V. microstoma* (Fig.4d), indicating a more constrained movement within the micro area. On the contrary, more spanned confinement ratio values, closer to one, were registered for *P. parasitica* zoospores farther from the potassium injection point (Fig.4b) and for *V. microstoma* motile forms (Fig.4d), representing a larger displacement along their tracked trajectories. Similarly, but with a slightest significant difference, at least for replicate 1 ($p = 0.0007$), *E. aerogenes* reported larger displacement for cells invested by *V. microstoma* sessile water flow and more

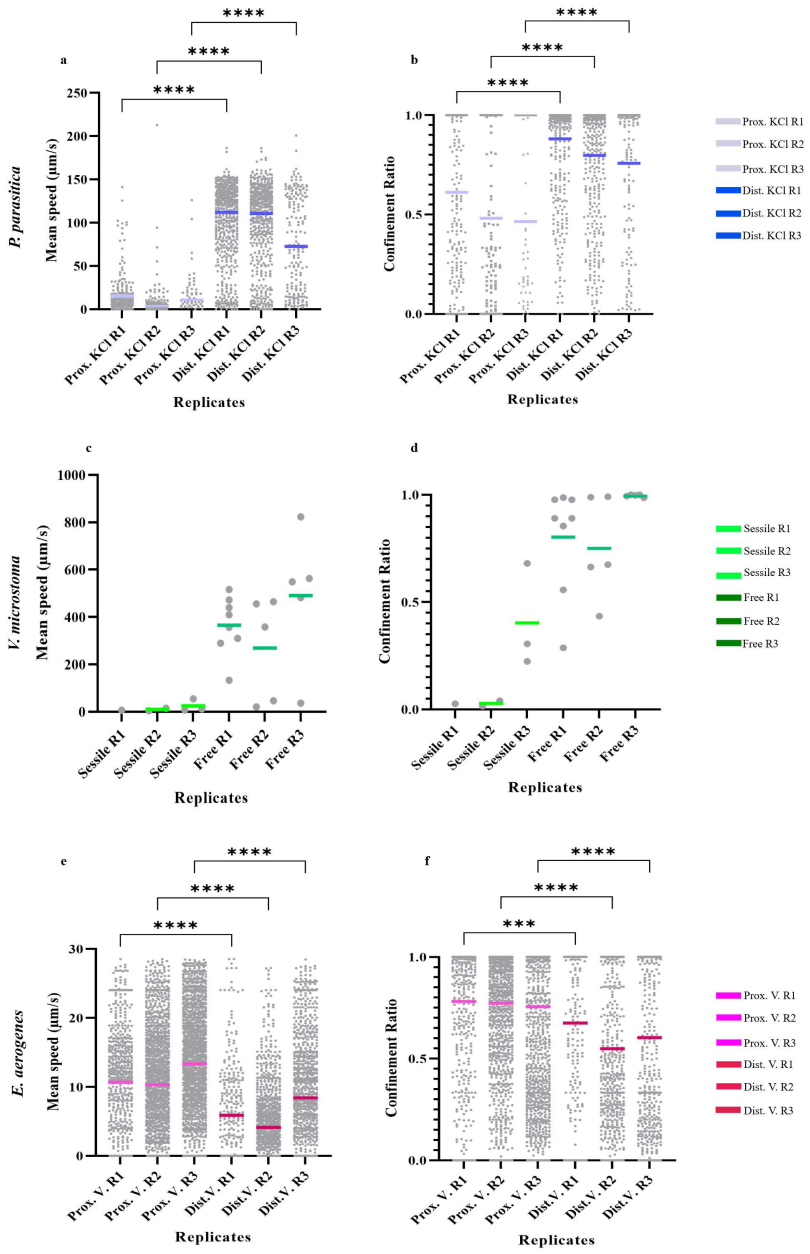

Fig. 4 Analysis of mean speed and confinement ratio in the six different defined micro-environments. (4a; 4b) *P. parasitica* zoospores proximal or distant from KCL injection point (total number of tracks: 453 and 1164 respectively). (4c;4d) *V. microstoma* fre-swimming forms (total number of tracks:18) vs *V. microstoma* sessile forms (total number of tracks: 6). (4e;4f) *E. aerogenes* proximal or distant from V (*V. microstoma* sessile forms) (total number of tracks: 4222 and 2588 respectively). *** and **** indicate a significant difference calculated by Sidak test between the two conditions considered in each replicate where ($p = 0.0007$) and ($p < 0.0001$).

constrained movement for cells far from sessile protozoa cells (Fig.4f).

Discussion

Prokaryotic and eukaryotic microorganisms possess the ability to respond to environmental

	Microbial Species	Micro-environment	Frames	Grid cells analyzed	Number of Spots	Number of Tracks
Replicate 1	*P. parasitica*	Proximal to KCI	[1-143]	A1-A2-A3	4248	231
		Distant from KCI	[1-143]	C1-C2-C3	3839	505
	V. microstoma	Sessile forms	[1-114]	A5-A6	114	1
		Free forms	[1-114]	C4-C5-C6	52	8
	E. aerogenes	Proximal to V	[1-81]	A5-A6	3626	661
		Distant from V	[1-81]	C3-C4	2234	332
Replicate 2	*P. parasitica*	Proximal to KCI	[1-143]	A1-A2	2758	166
		Distant from KCI	[1-143]	C3-C4	5123	480
	V. microstoma	Sessile forms	[1-43]	A4-A5	86	2
		Free forms	[1-43]	A4-A5	57	5
	E. aerogenes	Proximal to V	[1-143]	D3-D4*	10209	1580
		Distant from V	[1-143]	B1-B2	11742	1060
Replicate 3	*P. parasitica*	Proximal to KCI	[1-41]	A1-A2	552	56
		Distant from KCI	[1-41]	D2-D3	1044	179
	V. microstoma	Sessile forms	[1-25]	A1-A2	51	3
		Free forms	[1-25]	B5-C5	16	5
	E. aerogenes	Proximal to V	[1-143]	A1*	8727	1981
		Distant from V	[1-143]	B4-B5	6316	1196

Table 2 Replicates and corresponding micro-environment analyzed for the three microbial species. Micro-environments were identified using the grid cells illustrated in Figure 3. For each replicate and micro-environment, the three microbial species presented different numbers of spots and tracks detected. (*) in *E. aerogenes* microenvironment (Proximal to V) of Replicate 2 indicates that the considered grid cells include part of the underlying E3 and E4 cells; (*) in *E. aerogenes* microenvironment (Proximal to V) of Replicate 3 indicates that the considered grid cells include part of the above A1 cell.

clues. Detection and response to exogenous signals result in morphological, physiological and motility changes [26, 27]. In soil, multiple biotic and abiotic factors, including ion fluxes originating from plant root exudates or from the resultant of soil edaphic properties, mediate soil biota complex interactions within microbiota, and between microbes and plants [1, 28]. In recent years, the precise environmental control typical of microfluidic technologies coupled with automated cell tracking has begun to offer new opportunities to investigate and visualize the dynamics of telluric microbial species [6–8, 10, 11]. However, although these technologies have been already applied to screen single species realtime reactions to particular drivers, so far, no implementation has been developed to analyze the instantaneous impact of a driver on the behavior and interaction network of multiple microbial species within synthetic community like-systems.

In this article, we combine existing microfluidic technologies to improved automated cell tracking algorithms, to implement a method for the characterization and analysis of the dynamic

response of three different soil microbial species to a soil driver, potassium. At this aim, TrackMate algorithms [14] were applied to analyze recorded movies of a synthetic community formed by *Phytophthora parasitica* zoospores, *Vorticella microstoma* protozoa cells and *Enterobacter aerogenes* cells, confined in chambered coverslips. The method allowed to first accurately partition and morphologically characterize the three-cell species forming a simple synthetic community, and later to determine their specific motion response to the selected driver, and reveal further secondary interactions.

Morphological differences among the three different species were identified using a mask detector. Three categories of spots corresponding to the three microbial cells were differentiated according to size criteria (cell radius) and separately analyzed to retrieve morphometric parameters (here area and perimeter) (Fig. 2a-2b). The smaller group of detected cells (Table 1), here *V. microstoma* included the largest objects present in the mixed-suspension, identified either as ellipsoidal protozoa sessile trophont or circular telotroch forms (Fig.1d). On the other hand, the smallest microbial form detected, *E. aerogenes* bacteria was found to be the largest population (Table 1).

The three size-partitioned groups were then separately analyzed by the Nearest-neighbor tracker to determine cell-specific motion and behavior characteristics. Distribution analysis in response to the generated potassium gradient at millimetric scale revealed distinct motion dynamics for each species. Consistent with previous findings, the results confirmed the tendency of *P. parasitica* zoospores to adopt negative chemotaxis (Fig.1f), by moving toward micro-areas where potassium concentration is below the reported threshold range of 1-4 mM [11]. Accordingly, zoospores submitted to negative chemotaxis, moved with long linear trajectories and higher mean speed values in the microenvironment areas distant from the potassium inclusion point (Fig.3c) (Fig.4), while nearly immobile zoospores, corresponding to de-flagellated encysted zoospores, remained in proximity of potassium injection point (Fig.3c) (Fig.4). In line with previous observations, upon potassium treatment (5-10 mM) zoospores lose their flagella and consequently encyst [16]. No interference in the behavior of the zoospores by the two other species could be revealed reciprocally.

In a different way, sessile and free-swimming *V. microstoma* cells (with mean speed on average above 200 $\mu m/s$) (Fig.4c) resulted to not be affected by the potassium gradient, by uniformly distributing all around the millimetric investigated field (Fig.1g), regardless the proximity or not to the micro-areas with highest ion concentration (Fig.3). Contained mean speed and confinement ratio values, higher than 0 $\mu m/s$ and 0 respectively, for *V. microstoma* sessile forms

(Fig.2) (Fig.4c), were expected considering that stalk contractions in sessile forms might promote limited motility [17].

Also *Enterobacter aerogenes* cells millimetric distribution did not appear to be influenced by the generated potassium gradient, but rather affected by the presence of *V. microstoma* sessile forms (Fig.1h). The circular trajectories patterns observed in the immediate micro-environment of *V. microstoma* sessile forms differed from the ones described in micro-areas more distant from protozoa sessile forms (Fig. 3c). Higher mean speed recordings and confinement ratio rates (Fig. 4e-4f) resulted to be associated to *E. aerogenes* cells moving in proximity of *V. microstoma* sessile forms, as results of the advective water flow generated by the cilia contraction on the mouth-like part of *Vorticella* sessile zooid. In agreement with previous studies [17], we can state that in this particular case, *V. microstoma* sessile forms use the advective water flow to drag *E. aerogenes* cells as food particles for its nourishment, thus producing the observed circular vortexes. Although with lower mean speed and confinement ratio values (Fig.3c), bacterial cells distant from *Vorticella* sessile forms also appeared to move, with shorter and more linear trajectories. Considering that single *Vorticella* sessile forms can move microdiameter particles at least 450 μm away [17], we can assume that in our approximatively 1000*800 μm environment, with multiple protozoa sessile forms, even bacteria "distant" from *Vorticella* sessile forms are affected by their generated advective water flow, even if in a less spectacular form. This assumption was further confirmed by observing bacteria motion dynamics in isolated conditions (Additional File 5). In the absence of *Vorticella* sessile forms, *E. aerogenes* cells were either non-motile or exhibited confined movement with shorter and non-linear trajectories probably resulting from Brownian motion patterns, associated to relatively lower mean speed distribution compared to those recorded under mixed suspension conditions (Additional File 5; Adiitional File 6).

The results achieved so far demonstrate the efficiency of the implementation of the proposed method by offering the ability to characterize the behaviors of at least three species in a mixed suspension and their displacements in the milli- or micrometric environment considered. However, some limitations that need to be considered and further integrated emerged. A first set of constraints is related to the efficiency of morphological analysis that, in case of investigation of morphologically similar species, might be limited. In this case, other kinds of detection could be implemented. For example, morphologically similar species might fuse to different fluorescent markers, to be then easily detected and distinguished based on pixel intensity values. Another aspect of morphological-related limitations is related to

the estimation of cell shape. For very small-sized cells, such as bacteria, the shape associated to cells might change depending on the resolution of magnification adopted during microscopic observations. The image acquisition moment resulted to be a crucial step also for the adoption of the right thresholding values in the resulting output binary frames for further analyses. Since spots detection relies on spot-associated pixel definition, it is crucial to adopt the most suitable thresholding parameters. Here, threshold values were adjusted differently for each species in each replicate, leading to large intervals of morphological features (area and perimeter) in detected spots associated to the same species in different replicates (Fig. 2a-2b).

Conclusion

We have developed an optimized two-step approach for the efficient analysis of a mixed synthetic microbial suspension response to an external environmental driver. In this case, the approach first enabled us to identify and distinguish, based on morphological features, the three species we specifically cultured as a mixed suspension. In a second moment, it enabled us to describe the species-specific motion response to the potassium external driver, revealing a complex network of interactions not only between the species and their environment but also intra-species, in the specific the case of ciliate and bacteria cells.

Based on the results obtained, we can propose this as a valid and reproducible approach for the characterization at high-temporal scale of microbial communities dynamics and interaction with their environment. The advantage of this method is also supported by its low reproducible cost, considering that it is based on an image analysis step, using an open-source tool and prefabricated cost-effective microfluidic devices. We can thus imagine applying this approach as a supplementary tool to define properties of synthetic microbial community within soil water film, or other habitats like fresh-water ones. In these cases, such automated-tracking-based approach would enable the simultaneous analysis of different microbial species interactions. Similarly, in the field of plant disease management, the method might enable screening of potential biocontrol agents, by defining drivers' effect on co-distribution and interactions between pathogenic and beneficial microbial species and between biocontrol agents in the vicinity of host plant.

List of abbreviations.

- E = *Enterobacter aerogenes*
- KCl = Potassium chloride
- P = *Phytophthora parasitica*
- V = *Vorticella microstoma*

Supplementary information. The article has supplementary files.

Authors' contributions. CL, EG, AA, XN contributed to the conception of this work. CL, EG, PT develop the methodology. Formal analysis were performed by CL, EG, MK. Writing of the article was done by CL and EG. EG, AA, PT, CC, XN contributed to the concept and revised the manuscript. The work was supervised by EG, XN, AA. All authors have read and agreed to the published version of the manuscript.

Acknowledgments. We acknowledge Catherine Mura for technical assistance and Franck Panabieres for scientific discussion.

Funding. This work received support from the French government, managed by the French National Research Agency under the Investissements d'Avenir UCAjedi project bearing the reference n. ANR-15-IDEX-01. Carlotta A. Lupatelli received a PhD grant financed by the Graduate School LIFE, Graduate School SPECTRUM and Academy 4 (Université Côte-d'Azur). The work was also supported by the National Research Agency project n. ANR-22-CE20-0021.

Availability of data and materials. All generated or analyzed data are included in this published article and its additional files.

Declarations

Ethics approval and Consent to participate. Not applicable.

Consent for publication. Not applicable.

Competing interests. The authors declare they have no competing interests.

Supplementary information

The online version contains supplementary material available at url.

Additional file 1

Method workflow illustration. The workflow represents different steps of the image-based method for microbial mixed-suspension behavioral analysis.

Additional file 2

The original movie of microbial mixed-suspension (Replicate 1) is available in the link.

Additional file 3

The original movie of microbial mixed-suspension (Replicate 2) is available in the link.

Additional file 4

The original movie of microbial mixed-suspension (Replicate 3) is available in the link.

Additional file 5

Trajectories of isolated *E. aerogenes*.

Additional file 6

Motion and morphological description of isolated *E. aerogenes*.

References

[1] De Deyn GB, Kooistra L. The role of soils in habitat creation, maintenance and restoration. Philosophical Transactions of the Royal Society B. 2021;376(1834):20200170.

[2] Kuzyakov Y, Blagodatskaya E. Microbial hotspots and hot moments in soil: concept & review. Soil Biology and Biochemistry. 2015;83:184–199.

[3] Nannipieri P. Soil is still an unknown biological system. Applied Sciences. 2020;10(11):3717.

[4] Lauber CL, Ramirez KS, Aanderud Z, Lennon J, Fierer N. Temporal variability in soil microbial communities across land-use types. The ISME journal. 2013;7(8):1641–1650.

[5] Aufrecht J, Khalid M, Walton CL, Tate K, Cahill JF, Retterer ST. Hotspots of root-exuded amino acids are created within a rhizosphere-on-a-chip. Lab on a Chip. 2022;22(5):954–963.

[6] Bernier LS, Junier P, Stan GB, Stanley CE. Spores-on-a-chip: new frontiers for spore research. Trends in Microbiology. 2022;30(6):515–518.

[7] Bedekovic T, Brand AC. Microfabrication and its use in investigating fungal biology. Molecular Microbiology. 2022;117(3):569–577.

[8] Stanley CE, van der Heijden MG. Microbiome-on-a-chip: new frontiers in plant–microbiota research. Trends in microbiology. 2017;25(8):610–613.

[9] Davidson SL, Niepa TH. Micro-Technologies for Assessing Microbial Dynamics in Controlled Environments. Frontiers in Microbiology. 2022;12:4157.

[10] Massalha H, Korenblum E, Malitsky S, Shapiro OH, Aharoni A. Live imaging of root–bacteria interactions in a microfluidics setup. Proceedings of the National Academy of Sciences. 2017;114(17):4549–4554.

[11] Galiana E, Cohen C, Thomen P, Etienne C, Noblin X. Guidance of zoospores by potassium gradient sensing mediates aggregation. Journal of the Royal Society Interface. 2019;16(157):20190367.

[12] Schindelin J, Arganda-Carreras I, Frise E, Kaynig V, Longair M, Pietzsch T, et al. Fiji: an open-source platform for biological-image analysis. Nature methods. 2012;9(7):676–682.

[13] Tinevez JY, Perry N, Schindelin J, Hoopes GM, Reynolds GD, Laplantine E, et al. TrackMate: An open and extensible platform for single-particle tracking. Methods. 2017;115:80–90.

[14] Ershov D, Phan MS, Pylvänäinen JW, Rigaud SU, Le Blanc L, Charles-Orszag A, et al. TrackMate 7: integrating state-of-the-art segmentation algorithms into tracking pipelines. Nature Methods. 2022;19(7):829–832.

[15] Haro R, Benito B. The role of soil fungi in K+ plant nutrition. International journal of molecular sciences. 2019;20(13):3169.

[16] Appiah AA, Van West P, Osborne MC, Gow NA. Potassium homeostasis influences the locomotion and encystment of zoospores of plant pathogenic oomycetes. Fungal Genetics and Biology. 2005;42(3):213–223.

[17] Ryu S, Pepper RE, Nagai M, France DC. Vorticella: a protozoan for bio-inspired engineering. Micromachines. 2016;8(1):4.

[18] Weisse T, Jezberova J, Moser M. Picoplankton feeding by the ciliate Vorticella similis in comparison to other peritrichs emphasizes their significance in the water purification process. Ecological Indicators. 2021;121:106992.

[19] Davin-Regli A, Lavigne JP, Pagès JM. Enterobacter spp.: update on taxonomy, clinical aspects, and emerging antimicrobial resistance. Clinical microbiology reviews. 2019;32(4):e00002–19.

[20] Bitton G, Lahav N, Henis Y. Movement and retention of Klebsiella aerogenes in soil columns. Plant and Soil. 1974;40:373–380.

[21] D'alessandro M, Erb M, Ton J, Brandenburg A, Karlen D, Zopfi J, et al. Volatiles produced by soil-borne endophytic bacteria increase plant pathogen resistance and affect tritrophic interactions. Plant, cell & environment. 2014;37(4):813–826.

[22] Galiana E, Marais A, Mura C, Arbiol G, Ponchet M. Ecosystem screening approach for pathogen-associated microorganisms affecting host disease. Applied and Environmental Microbiology. 2011;77(17):6069–6075.

[23] Larousse M, Rancurel C, Syska C, Palero F, Etienne C, Nesme X, et al. Tomato root

microbiota and Phytophthora parasitica-associated disease. Microbiome. 2017;5(1):1–11.

[24] Larousse M, Govetto B, Séassau A, Etienne C, Theodorakopoulos N, Deleury E, et al. Characterization of PPMUCL1/2/3, three members of a new oomycete-specific mucin-like protein family residing in Phytophthora parasitica biofilm. Protist. 2014;165(3):275–292.

[25] De Pascalis C, Pérez-González C, Seetharaman S, Boëda B, Vianay B, Burute M, et al. Intermediate filaments control collective migration by restricting traction forces and sustaining cell–cell contacts. Journal of cell biology. 2018;217(9):3031–3044.

[26] Wu D. Signaling mechanisms for regulation of chemotaxis. Cell research. 2005;15(1):52–56.

[27] Iglesias PA, Devreotes PN. Navigating through models of chemotaxis. Current opinion in cell biology. 2008;20(1):35–40.

[28] Naylor D, McClure R, Jansson J. Trends in microbial community composition and function by soil depth. Microorganisms. 2022;10(3):540.

Supplementary Files

This is a list of supplementary files associated with this preprint. Click to download.

- Additionalfile1.pdf
- Additionalfile2.avi
- Additionalfile3.avi
- Additionalfile4.avi
- Additionalfile5.pdf
- Additionalfile6.pdf